# Phase-controlling phononic crystals: Realization of acoustic Boolean logic gates

S. Bringuier[a] and N. Swinteck
*Department of Materials Science and Engineering, University of Arizona, Tucson, Arizona 85721*

J. O. Vasseur and J.-F. Robillard
*Institut d'Electronique, de Micro-électronique et de Nanotechnologie, UMR CNRS 8520, Cité Scientifique, 59652 Villeneuve d'Ascq Cedex, France*

K. Runge, K. Muralidharan, and P. A. Deymier
*Department of Materials Science and Engineering, University of Arizona, Tucson, Arizona 85721*

(Received 28 April 2011; revised 27 July 2011; accepted 8 August 2011)

A phononic crystal (PC) consisting of a square array of cylindrical Polyvinylchloride inclusions in air is used to construct a variety of acoustic logic gates. In a certain range of operating frequencies, the PC band structure shows square-like equi-frequency contours centered off the Gamma point. This attribute allows for the realization of non-collinear wave and group velocity vectors in the PC wave vector space. This feature can be utilized to control with great precision, the relative phase between propagating acoustic waves in the PC. By altering the incidence angle of the impinging acoustic beams or varying the PC thickness, interferences occur between acoustic wave pairs. It is recognized that information can be encoded with this mechanism (e.g., wave amplitudes/interference patterns) and accordingly to construct a series of logic gates emulating Boolean functions. The NAND, XOR, and NOT gates are demonstrated with finite-difference time-domain simulations of acoustic waves impinging upon the PC.
 [DOI: 10.1121/1.3631627]

PACS number(s): 43.40.Fz, 43.20.Fn, 43.20.El, 43.20.Gp [ANN] Pages: 1919–1925

## I. INTRODUCTION

Phononic crystals (PCs), the acoustic analog to photonic crystals, are periodic, composite structures composed of materials with differing elastic properties. The utility of PCs are their ability to modify phonon dispersion through multiple scattering processes or local resonances.[1,2] Over the past 10 yr, PCs have been designed to show a variety of useful properties particular to spectral ($\omega$-space) and wave vector ($k$-space) functions. Spectral functions result from band gaps in the transmission spectra for stopping phonons or narrow passing bands for filtering.[3–5] Wave vector functions result from refractive characteristics linked to passing bands such as those exhibiting negative indices of refraction, zero-angle refraction (e.g., wave collimation) or indices of refraction that are dependent on incidence angle.[6–8] Other functions, such as wave-guiding and mode localization, have been demonstrated in defected phononic structures.[9] Recently, progress has been made in the extension of the properties of PCs beyond the $\omega$-$k$ space and into the space of acoustic wave phase ($\varphi$-space).[10,11] The relative phase between pairs of acoustic waves propagating in a PC medium can be fully understood with analysis of the PC band structure and equi-frequency contours (EFCs). It was demonstrated that PCs showing EFCs with non-collinear wave and group velocity vectors are ideal systems for controlling the relative phase between propagating acoustic waves on account of the fact that excited Bloch modes within the PC travel at different phase velocities.[11] In this situation, the relative phase between waves can be precisely modulated by either changing the incident angles of the incoming acoustic beams (i.e., changing the phase velocity at which the beams travel in the PC) or varying the thickness of the PC. In addition to this feature is another phase property of PCs stemming from having the EFC of the incident homogeneous medium being larger than the first Brillouin zone of the PC. In this instance, the same Bloch modes can be excited within the wave vector space ($k$-space) of the PC by incident waves with different incident angles. Impinging beams with this characteristic are referred to as complementary angle inputs or complementary waves.[11] The complementary waves travel the same path within the PC (i.e., the path consistent with the angle of refraction) and, upon exiting the PC, contribute to beam splitting.[10,11] Altering the relative phase between the incident beams changes the manner at which these modes superpose within the PC. Specifically, if two complementary waves enter the PC out of phase, then along the path of the refracted beam, destructive interference will cancel out the amplitudes of the propagating waves. These PCs, which have distinctive phase-properties, can greatly enrich the field of phononics. PCs with full spectral, wave-vector, and phase-space properties ($\omega$, $k$, and $\varphi$) have the potential of impacting a broad range of technologies. Past efforts in developing acoustic devices utilizing PCs with just spectral or refractive properties have led to inherently passive designs. Adding the dimension of phase-control enhances

[a]Author to whom correspondence should be addressed. Electronic mail: stefanb@email.arizona.edu

the functionalities of PCs and can lead to more active acoustic based technologies.

Here we utilize the above-mentioned phase phenomena in a two dimensional PC to develop a new paradigm in acoustic wave based Boolean logic functions. This model offers precise control of phase between acoustic waves within a finite volume of PC. To the best of our knowledge, this is the first report of acoustic based logic functions based on the control of phase of acoustic waves using a PC. Past work in acoustic wave based logic devices utilized the addition or subtraction of out-of-phase sources;[12] however, this work did not include the use of a PC. Other work in photonic crystals, utilized non-linear effects in the temporal transmission spectra.[13,14] The work presented here constitutes a significant effort to broaden the functions of two-dimensional (2D) PCs. This paper is organized as follows: In Sec. II, we derive an analytical model for controlling the phase between acoustic waves propagating through a PC. Additionally, we briefly describe the finite-difference time-domain (FDTD) method and its application to simulating acoustic based Boolean logic gates, specifically, the NAND, XOR, and NOT functions. Results of the FDTD simulations are reported in Sec. III. Conclusions are drawn in Sec. IV.

## II. MODEL AND METHODS

### A. PC band structure and EFCs

The 2D PC consists of square array of PVC cylinder inclusions embedded in an air matrix. The lattice parameter is $a = 27.0$ mm and the radius of the inclusions is $r = 12.9$ mm [see Fig. 1(a)]. The physical parameters of the constitutive materials of this PC are: $\rho_{pvc} = 1\,264$ kg/m$^3$, $C_{t,pvc} = 1\,000$ m/s, $C_{l,pvc} = 2\,300$ m/s, $\rho_{air} = 1.3$ kg/m$^3$, $C_{t,air} = 0$ m/s, and $C_{l,air} = 340$ m/s, where $\rho$ is the mass density, $C_t$ is the transverse speed of sound, and $C_l$ is the longitudinal speed of sound.

The FDTD technique used in this work is based on the discretization of the elastic wave equation; therefore to simulate materials other than solid, it is necessary to approximate the transverse speed of sound to be zero for those materials. The band structure and EFCs for the infinite, periodic PC is calculated with the plane wave expansion (PWE) method.[15] This numerical scheme replaces the elastic wave equation with an eigenvalue problem by taking the Fourier expansion of the elastic displacement field and the physical parameters of the constituent materials along reciprocal lattice vectors. The PVC cylinders are considered infinitely rigid and of infinite height. The assumption of rigidity simplifies the band structure calculation and is enabled by a large contrast in density and speed of sound between the solid inclusions and the matrix medium. The 441 reciprocal space vectors were utilized to ensure convergence on the solution. The resulting band structure can be seen in Fig. 1(b). The frequency range 13.5-17.0 kHz (fourth band) shows a partial band gap in the ΓX direction. We note that the group velocity is the gradient of the $\omega(k)$ dispersion surface and for the fourth passing band this surface is "pyramid-shaped" and should have positive and negative group velocities. The EFC corresponding to 13.5 kHz is shown in Fig. 1(c). The contours are not centered on the Γ point, which is consistent with the partial band gap

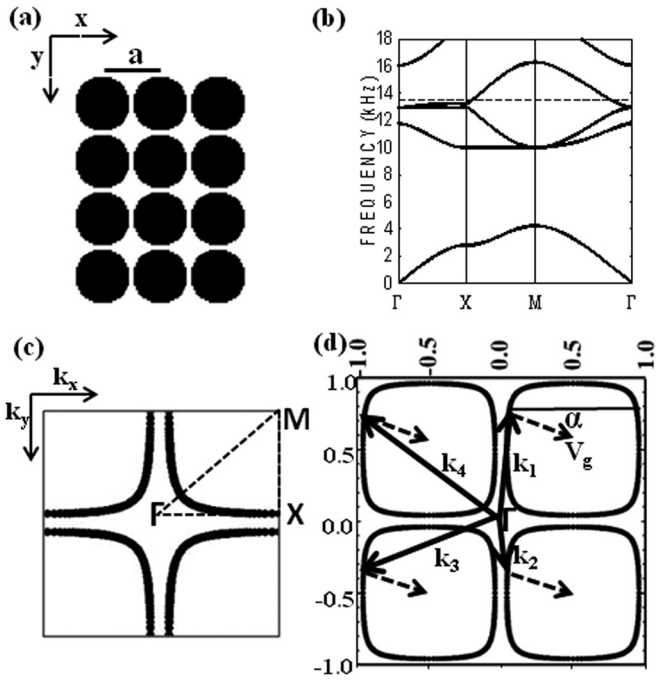


FIG. 1. (a) Structure of PVC-air phononic crystal (PC) with lattice parameter $a = 27$ mm. (b) Band structure with principal directions of propagation in first Brillouin zone for PVC-air system, dashed line at 13.5 kHz. (c) Corresponding EFC of the first Brillouin zone that is not centered about the Gamma point. (d) Extended zone scheme of equi-frequency contours (EFC) of the PC. All associated wave vectors with a given Bloch mode are shown. Group velocity vector is not collinear with wave vectors and has angle α with horizontal axis.

seen along the ΓX direction in this frequency range. An extended zone scheme of the first Brillouin zone is shown in Fig. 1(d) for 13.5 kHz. One can see the square-like shape of these contours with this representation. Other pass bands in this system, which result in nearly square EFCs and are not centered about the Γ point but on the M point, will exhibit these phenomena needed to construct logic gates.

This diagram is particularly useful in understanding wave propagation in PCs. The extended zone scheme of the EFC in Fig. 1(d) is used in this paper to analyze waves propagating in the PVC-air PC implanted in an air enclosure. This representation highlights the various Bloch modes of the PC that will be excitable by incident acoustic waves with wave vectors exceeding the size of the first Brillouin zone. We make a quick remark about other exciting wave vectors. These waves are a result of the excitation of Bloch modes in the PC. For this system, it so happens that the EFC of air is twice as large as the PVC-air crystal. The result of this is beam splitting with angle dependent amplitude. In spite of the beam splitting, we choose to focus our attention on the output side of a PC to wave vectors $\mathbf{k_1}$ [see Fig. 1(d)] pointing upward.

### B. Phase control using a PC

In this subsection, we will briefly review the phase-controlling properties of the PVC-air PC that have been demonstrated by Swinteck *et al.*[11] The phase of acoustic waves propagating through a finite thickness crystal (thickness $d$) arises from the fact that the group velocity and the wave vector are not collinear [see Fig. 1(d)]. The group velocity vector

is oriented along the gradient of the EFC, which is the direction of energy propagation. The wave vector inside the PC originates at the Gamma point and ends on the EFC where its parallel component is that of the incident wave. The direction of the wave vector is specified by the phase velocity. Let us consider a Bloch wave with wave vector $\boldsymbol{k}$, the path traveled in the PC by the wave is:

$$\vec{R} = d\hat{\imath} + d\ tan(\alpha)\hat{J} \tag{1}$$

Where $i$ and $j$ are unit vectors in the horizontal ($x$) and vertical ($y$) directions, respectively, and $\alpha$ is the angle the group velocity makes with the horizontal axis. We now take into account two non-complementary waves with wave vectors, $\boldsymbol{k}$ and $\boldsymbol{k}'$ (i.e., different group velocities, $\alpha$), entering the PC at the same location. These two waves do not excite the same Bloch modes in the PC and therefore will travel paths of different length and direction. This path difference is due to the non-collinear group velocity and wave vector, and causes the two waves to exit the PC at different locations and exhibit relative phase shift. To calculate the phase shift in the PC between these two waves, we first write their spatial form when they exit as:

$$e^{i}(\vec{k}\cdot\vec{R}) = e^{i\frac{2\pi}{a}d\left\{k_x\hat{\imath}+tan(a)k_y\hat{J}\right\}} \tag{2}$$

$$e^{i}(\vec{k}'\cdot\vec{R}') = e^{i\frac{2\pi}{a}d\left\{k'_x\hat{\imath}+tan(a')k'_y\hat{J}\right\}} \tag{3}$$

Where $\boldsymbol{R}$ and $\boldsymbol{R}'$ are the path traveled by the two waves in the PC given by Eq. (1). The difference in the argument of the real parts for the two waves (i.e., phase shift) is therefore given by:

$$\begin{aligned}\Phi_{k,k'} &= \left(\vec{k}\times\vec{R}\right) - \left(\vec{k}'\times\vec{R}'\right) \\ &= \frac{2\pi}{a}d\left\{k_x\hat{\imath} + tan(\alpha)k_y\hat{J} - k'_x\hat{\imath} - tan(\alpha')k'_y\hat{J}\right\}\end{aligned} \tag{4}$$

From Eq. (4), the thickness, $d$, of the crystal plays an integral part in the phase shift between waves in the PC.

In Fig. 2(a), the EFCs of air and the PC with two acoustic waves in air incident upon the crystal and then exiting to air. The wave vector that is parallel to the surface of the PC is conserved when entering and exiting the crystal. In this figure, the direct space diagram displays the phase shift that occurs between two non-complementary waves incident from air on to the same point of the PC [see Fig. 2(b)]. Utilizing Eq. (4), it can be shown that a phase shift will occur in the PC between the two waves. This phase shift is preserved and upon exiting the crystal the two waves will cross paths where the vectors $\boldsymbol{R}_{out}$ and $\boldsymbol{R}'_{out}$ intersect [see Fig. 2(a)]. These different paths lead to an additional phase shift which is given by the first difference in Eq. (5).

$$\begin{aligned}\Phi_{total} &= \left(\vec{k}_{out}\cdot\vec{R}_{out}\right) - \left(\vec{k}'_{out}\cdot\vec{R}'_{out}\right) \\ &+ \left(\vec{k}\cdot\vec{R}\right) - \left(\vec{k}'\cdot\vec{R}'\right)\end{aligned} \tag{5}$$

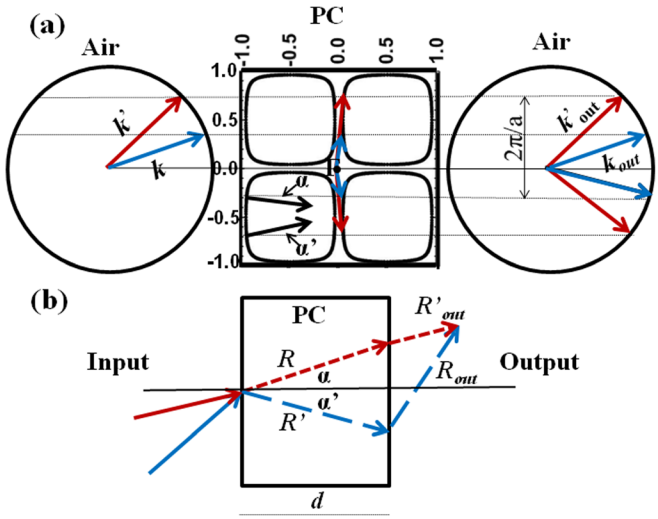


FIG. 2. (Color online) (a) EFC diagram of PVC-air PC embedded in air. Two different wave vectors, $\boldsymbol{k}$ and $\boldsymbol{k}'$, are incident on the left surface of the crystal. These two incident waves do not excite the same Bloch modes inside the PC and therefore have group velocity vectors with different angles, $\alpha$ and $\alpha'$ (b) In direct space, there is a phase shift between $\boldsymbol{k}$ and $\boldsymbol{k}'$ due the different paths, $\boldsymbol{R}$ and $\boldsymbol{R}'$ traveled in the PC as well as the paths traveled outside the PC. Beam splitting occurs but is not shown in direct space for simplicity.

Thus non-complementary waves that travel from the input side, through the PC, and exit on the output side, will cross paths at some distance to constructively or destructively interfere. This allows for the ability to encode information in the amplitude of incident non-complementary acoustic waves and operate on through interference.

We now consider two complementary waves with wave vectors, $\boldsymbol{k}$ and $\boldsymbol{k}'$, incident on the same location on the surface of the PC slab. These two complementary waves excite the same Bloch modes inside the PC. This situation is illustrated in Fig. 3(a); because the two waves excite the same

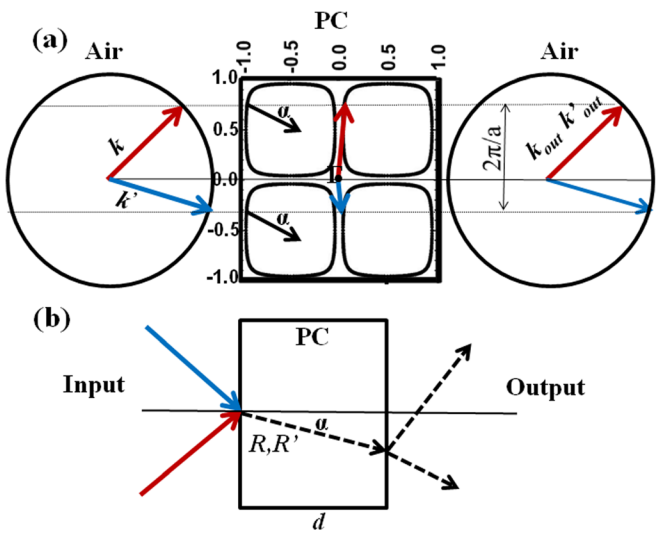


FIG. 3. (Color online). (a) EFC diagram for two different wave vectors, $\boldsymbol{k}$ and $\boldsymbol{k}'$, incident on the left surface of the PC that excite the same Bloch modes (i.e., matching group velocity angle $\alpha$). (b) In direct space, both waves experience identical paths traveled and will therefore superimpose in direct space and exit along the same point of the PC (Beam splitting is shown in direct space).

Bloch modes, their group velocity vectors are identical (e.g., same refraction angle $\alpha$) and therefore will occupy the exact volume in the PC. As a result of this, the two waves will follow an identical path as they propagate through the crystal [see Fig. 3(b)]. Thus, according to Eq. (4), there is no phase shift between complementary waves inside the crystal. It is also necessary to note that the waves inside the crystal retain the phase difference that may have been imposed on the incident acoustic waves prior to entering the PC. Subsequently by controlling the phase difference between these two complementary waves, one may obtain constructive or destructive interferences inside the PC. Destructive interference will lead to a condition for which there is no propagation through the crystal. On the other hand, constructive interference will allow for acoustic waves to travel through the PC. Similarly to the case of non-complementary inputs, we now arrive at the capability to encode information within the amplitude of incident complementary acoustic waves and operate on this information via interference.

### C. Method for the simulation of PC functions

Simulations of the Boolean logic functions that can be generated using a finite size phase-controlling PC are carried out by the FDTD, a method that has been extensively employed within the field of PCs.[16,17] The FDTD method discretizes the elastic wave equation in both time and space on a finite mesh. To ensure stability and convergence, courant conditions were used with a time step of $7.92e^{-7}$ seconds and cell size $dx = dy = a/30$. The PC is placed in an environment of air and the entire computational space was removed of any reflections and artifacts by the use of first order Mur absorbing boundary conditions on all sides of the simulation space.[18] In all the calculation reported in this paper, we have used a PC slab composed of a minimum of 23 periods in its thickness ($x$-direction) and 46 periods in its length ($y$-direction). The thickness and length are sufficient to ensure that the properties of the finite crystal approach those of the infinite crystal determined by the PWE method.[11] The sources and inputs in the simulation are composed of a diagonal line segment of nodes that vibrate with a given forcing function. The length of the sources and inputs is sufficiently large to minimize the spread of angles, mimicking plane wave behavior. The sources and inputs may acquire any incident angle to the face of the crystal that correspond with the nearly flat portion of the EFC (i.e., angles from 10° to 50°), other angles will be reflected due to the partial band gap or will undergo too large of angles of refraction inside the PC to be useful for construction of the devices. The sources and inputs are also given initial wave phase relations. On the output side of the simulated system we locate a detector, $D$.

## III. RESULTS AND DISCUSSION

In this section, we present the design of logic gates using the PVC-air PC and display the FDTD simulations for the NAND, XOR, and NOT gates. In these simulations, the displacement fields were obtained and used to validate the possibility of achieving Boolean logic functions using propagation and interference between waves impinging on a PC.

### A. NAND gate

The NAND gate is identified as a universal logic gate. Networks of universal gates such as the NAND gate can produce any of the other Boolean logic functions (i.e., all other gates).[19] The NAND gate function consists of two inputs that are operated on by the gate to produce one output. To construct the NAND gate, a PC with two non-complementary plane wave sources, $S_1$ and $S_2$, is impinging onto the crystal at fixed angles. These angles are 10° and 38° with their centers incident upon the same point of the crystal. The two sources are oscillating in-phase on the input side of the PC. The calculated total phase shift on the output side is $2\pi$ radians by use of Eq. (5). This total phase shift results in constructive interference on the output side between the centers of the exiting beams. In the simulation space, the point of intersection between the centers of the exiting beams occurs at 410 mm in $y$-direction and 1 550 mm in $x$-direction. The detector, $D$, is centered about this point and angled at 24° (10° + 38°/2) with a spatial width of 80 mm. Inputs, $I_1$ and $I_2$, for this system are the corresponding complementary waves to the sources, $S_1$ and $S_2$, respectively. Each input is set $\pi$ radians out of phase with the corresponding source to ensure destructive interference within the PC. These inputs are −19° and −50°, and their centers are incident upon the same point on the surface of the crystal as the sources. The inputs are turned on or off to obtain the input identifiers *1* and *0*, respectively. On the output side, the value of the average pressure where the exiting beams intersect on the detector $D$ is relative to a threshold and given the output identifiers *0* or *1*. The average pressure is defined as the time average of the absolute value of the pressure over one period. A schematic of the operation for the NAND gate is displayed in Fig. 4(a).

In Figs. 4(b) to 4(e), the resulting displacement field and corresponding average pressure at the detector are shown for the various cases. The point where the exiting beams intersect on the detector is highlighted by the dotted line. In Fig. 4(b), the inputs are turned off ($I_1 = 0$, $I_2 = 0$), which allows for the waves produced by the sources to travel through the PC and exit on the output side. The exiting beams destructively interfere where they intersect and a maximum average pressure is given the identifier *1*. To establish the system threshold, we observe the case for which the average pressure is at a minimum. In Fig. 4(e), the inputs are turned on ($I_1 = 1$, $I_2 = 1$), these inputs destructively interfere with the $S_1$ and $S_2$ in the PC. The resulting output is the lowest for all other input cases, and for this reason, it is used as the system threshold by assigning the identifier *0*. In Figs. 4(c) and 4(d), one may see that the output of the average pressure at the center of $D$ is above that of the threshold; in both instances, the identifier *1* is assigned. The displacement field and average pressure results for the NAND gate demonstrate the interference between complementary and non-complementary waves.

### B. XOR gate

In this subsection, we discuss the construction and results for the XOR gate. Although the XOR is not a universal logic gate, it remains important in most logic gating applications. The XOR gate operates similarly to the NAND

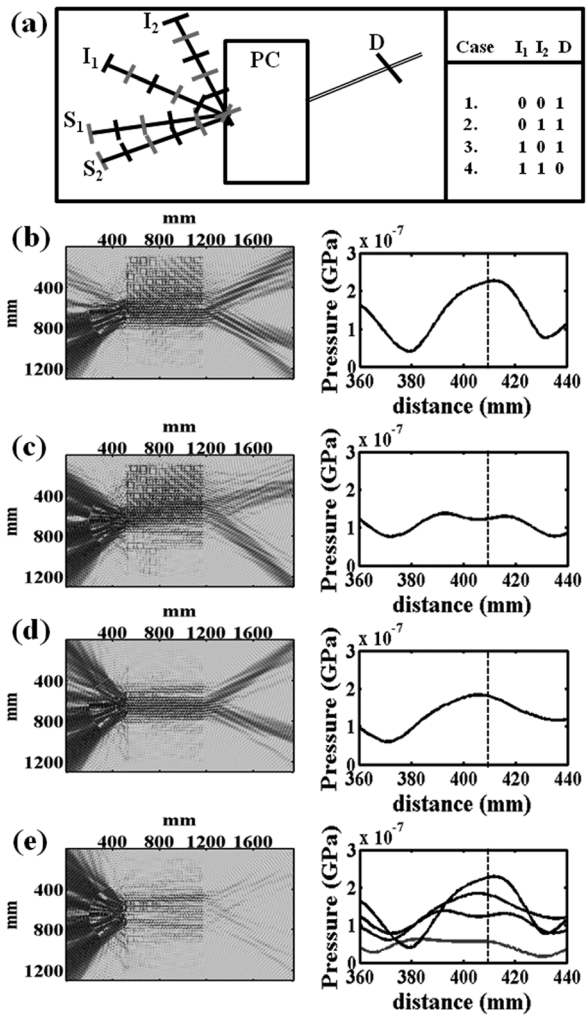


FIG. 4. (a) Schematic for NAND gate with corresponding truth table. (b) to (e) Finite-difference time-domain (FDTD) results for NAND gate construction. (b) Both inputs are turned on ($I_1$, $I_2 = 0$).On the output side, the time average of the absolute value of the pressure over one period (average pressure) is acquired at $D$, and the intersection between exiting beams (dashed line, 410 mm $y$-direction), is given the identifier *1*. (c) $I_1$ is on and $I_2$ is off. Complementary waves, $S_1$ and $I_1$, destructively interfere within PC leaving non-complementary wave to exit, output result is *1*. (c) $I_1$ is off and $I_2$ is on, only non-complementary waves exit, output result is *1*. (d) Both inputs are turned on ($I_1$, $I_2 = 1$) and destructively interfere with sources, output result is *0* (light gray line).

gate with two inputs into the system and one output. For the XOR gate system, the sources, $S_1$ and $S_2$, consist of two non-complementary plane waves incident upon the same point of the crystal. The sources remain in phase with one another and their incident angles are fixed at 10° and 28.1°. The calculated total phase shift for exiting beams on the output side is $\pi$ radians given by Eq. (5). This occurs in the simulation cell at the location of 383 mm in the $y$-direction and 1 888 mm in the $x$-direction. The detector $D$ is centered about this point and given an angle of 19° (10° + 28.1°/2) with a spatial width of 80 mm. The inputs for the system consist of $I_1$ and $I_2$, which are the complementary waves of $S_1$ and $S_2$, respectively, and are out of phase by $\pi$ radians. The incident angles for $I_1$ and $I_2$ are fixed at angles −50° and −28.1° with their centers incident upon the same point as the sources. As in the NAND gate, the inputs are controlled and the output is compared to a threshold. A schematic of the XOR is shown in Fig. 5(a).

In Figs. 5(b) to 5(e), the displacement field and average pressure at $D$ is displayed for all input cases. In Fig. 5(b), one may see that both inputs are turned off ($I_1 = 0$, $I_2 = 0$), permitting both sources exit the PC. The average pressure at $D$ is shown, and there is a phase shift between exiting beams giving rise to destructive interference at the point where they intersect. As was done in the NAND gate, the threshold for the average pressure is identified. Because cases one and four will have outputs of 0 [see Fig. 5(a)], the one with the largest minimum average pressure is used to establish the system threshold. In case four, both inputs are turned on ($I_1 = 1$, $I_2 = 1$), and the resulting average pressure output is larger than that of case one; for this reason, it is used as the system threshold. In Figs. 5(c) and 5(d), case two ($I_1 = 0$, $I_2 = 1$) and case three ($I\text{-}_1 = 1$, $I_2 = 0$) show that the complementary inputs destructively interference inside the PC with the corresponding sources. The comparison between the

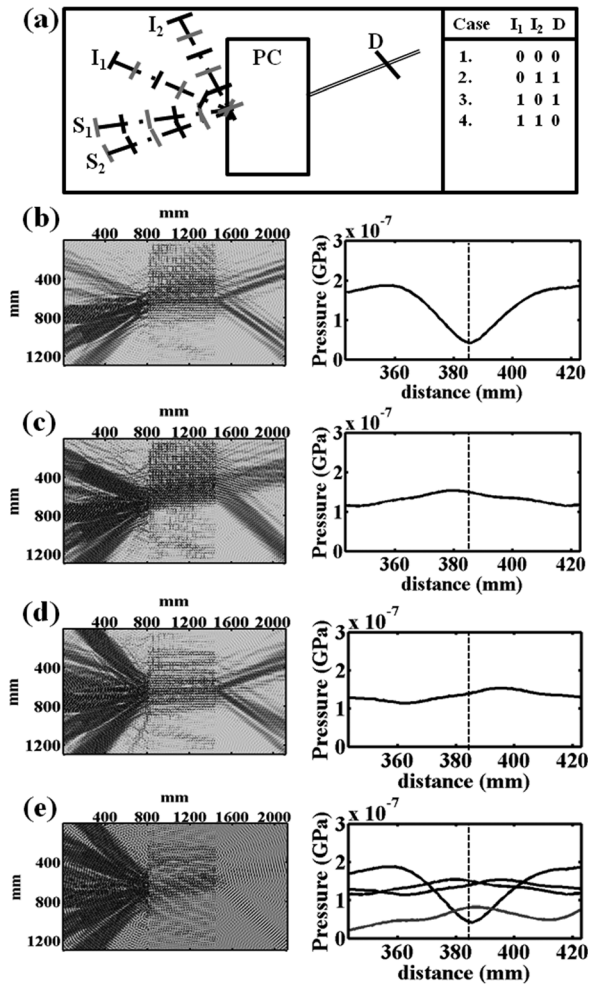


FIG. 5. (a) Schematic for XOR gate with corresponding truth table. (b) to (e) FDTD results for XOR gate construction (a). Both inputs are turned off ($I_1$, $I_2 = 0$). On the output side, average pressure at the detector $D$ is recorded. The intersection of exiting waves (dotted line, 383 mm $y$-direction) is given the identifier *0*. (b) $I_1$ is on and $I_2$ is off. Complementary waves destructively interfere within PC leaving non-complementary waves to exit, output result is *1*. (c) $I_1$ is off and $I_2$ is on, only non-complementary waves exit, output result is *1*. (d) Both sources are turned on ($I_1$, $I_2 = 1$) and complementary waves destructively interfere; output result is *0*.

NAND and XOR logic gates demonstrates the usage of a phase-controlling between non-complementary waves by the PC; this is because the first case for each gate is inherently different and thus the PC must operate on the inputs accordingly.

At this point, we interject that there is substantial energy loss for incident acoustic beams at the interface between the air and the PC. This loss is incident angle dependent and due to reflections. As a consequence of this, complementary waves will not undergo the same loss of energy at the interface with one exemption. This does not affect the interference within the PC for angle 28.1° (i.e., zero angle refraction) because the complementary wave is −28.1°, and therefore the loss of energy is equivalent.

### C. NOT gate

Similar to the XOR gate, the NOT gate remains important in logic gating applications. The NOT gate operates on one input and produces one output. For this reason, the construction of the NOT gate disregards the phase shift between non-complementary waves but instead implements the interference of complementary waves. The NOT gate system is composed of a source, $S_1$, and input, $I_1$. The source is a plane wave incident upon the PC and is set in a fixed angle of 28.1° and phase. The input for this system is the complementary plane wave of the source and is set at −28.1° and $\pi$ radians out of phase with $S_1$. The input is turned off and on accordingly [see Fig. 6(a)]. Because this gate does not operate on non-complementary beams, the detector is angled at 28.1° on the output side and centered about the exiting beam (538 mm in the $y$-direction and 1 753 mm in the $x$-direction). The threshold for the system is determined by the output for case two because its average pressure reading will be the lowest. In Fig. 6(b), the resulting displacement field and average pressure at $D$ are displayed. In this case, the input is turned off ($I_1 = 0$), and the resulting average pressure at the detector results in an identifier *1*. In the second case, the input is turned on ($I_1 = 1$) and interferes destructively with the source inside the PC; this is shown in Fig. 6(c). From the latter, a minimum average pressure is detected and the output is given the identifier *0*. As stated in the previous section, for angles 28.1 and −28.1, there is an equal loss of energy at the interface of the air and PC system. For this reason, one may see in Fig. 6(c) that the displacement field on the output side is roughly nonexistent.

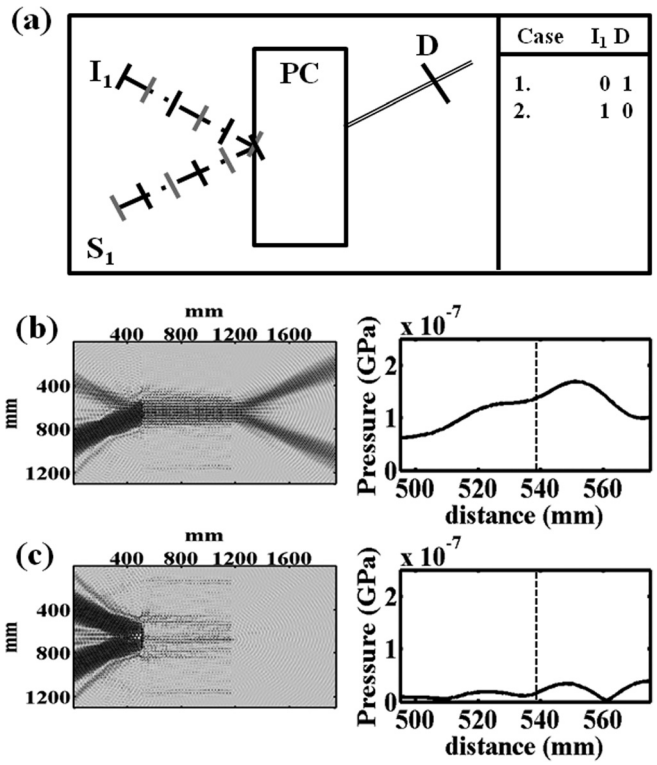


FIG. 6. (a) Schematic for NOT gate with corresponding truth table. (b) to (e) FDTD results for NOT gate construction (a). The input is turned off. On output side the average pressure at the detector $D$ is recorded. The center of the exiting wave (dotted line, 538 mm $y$-direction) is given the identifier *0*. (b) $I_1$ is turned on and destructively interferes with $S_1$ inside the PC; the output result is *1*.

### D. Device sensitivity

In this study, the operating frequency of 13.5 kHz was chosen because of the approximately perfect square EFC. However, for phase control, one does not have to have a nearly perfect square EFC. In the work done by J. Bucay *et al.*,[10] the operating frequency of 14.1 kHz was studied for the PVC-air system, and it was shown that the resulting EFC was nearly square in shape as well. Because the EFC does not change overall shape for a broad range of frequencies around 13.5 kHz (i.e., 13.5-16.5 kHz), the construction of the devices should maintain proper operation.

## IV. CONCLUSION

In this paper, we employ a PC that enables control of the phase for acoustic waves to implement Boolean logic functions through interferences. This PC is composed of polyvinylchloride cylinders in an air matrix with a lattice parameter $a = 27$ mm and a radius $r = 12.9$ mm. The phase-controlling is achieved through the features of the PC's band structure and, namely, its nearly square EFC at a frequency of 13.5 kHz. For this case, the wave vectors of Bloch modes are not collinear with the group velocity vectors. The result of this is a phase shift inside the PC for incident acoustic waves. It is important to note that these conditions are not limiting because, for a PVC-air PC, any combination of lattice parameter and radius that results in a filling fraction of $f = 0.7171$ will give rise to nearly square EFCs at some operating frequency. Furthermore, waves with different incident angles that do not excite the same Bloch modes (non-complementary waves) in the PC will exit on the output side and converge at some point to constructively or destructively interfere. In addition, the fact that the EFC of acoustic waves in the medium in which the PC is embedded is larger than the first Brillouin zone of the crystal enables the excitation of multiple Bloch modes. One can therefore take advantage of the spatial overlap of these modes (complementary waves) to achieve constructive and destructive interferences.

It is demonstrated with the FDTD that the unique temporal, spectral, and phase properties of this PVC-air PC can be utilized to showcase linear Boolean logic operations.

With this scheme, the NAND, XOR, and NOT logic gates are demonstrated. In addition, this method may be furthered adapted in a network of PCs to construct all other gates and perhaps an all acoustic logic circuit. The main advantage of these gates is that they rely on linear behavior of the acoustic materials. This linearity, however, requires that the acoustic logic gate device possesses at least a permanent source that can interfere with a corresponding input. In addition, this source has to be out of phase with respect to the input. The linearity of the Boolean function requires also system identified thresholds. These thresholds, however, may not be universal; that is, they may depend on the circuit in which a particular gate of interest is inserted. A possible remedy to this issue is to pass any input through a beam splitting PC (e.g., PVC-air). One of these beams serves as an input for a given gate, and the other beam subsequently serves as a reference. Instead of using absolute values of pressure as thresholds, one then would define thresholds relative to the pressure of the reference beam. In spite of these potential draw backs, the present work is still a significant step forward in the design of acoustic devices with higher functions (logic functions) based on PCs.

The Boolean logic functions presented in this paper rely on the phenomenon of Bragg scattering of acoustic waves by a periodic array of PVC inclusions. Imperfections in the periodicity of the array as well as defects in the PC may lead to degradation of the operating conditions of the logic gates. In the work done by J. Bucay *et al.*,[10] experimental measurements of the transmission of acoustic waves through a PVC-air PC were reported. In that study, great care was taken to fabricate a periodic structure; however, in spite of very small deviations (less than 1%) in position and alignment of the PVC cylinders, experimental and FDTD calculated transmissions showed very good agreement. It is therefore anticipated that the Boolean logic gates studied require as periodic a PC as possible but small imperfections may not impact its operation significantly.

## ACKNOWLEDGMENT

We gratefully acknowledge support from National Science Foundation Grant 0924103

[1]M. Sigalas and E. Economou, "Band structure of elastic waves in two dimensional systems," Solid State Commun. **86**(3), 141–143 (1993).

[2]J. O. Vasseur, B. Djafari-Rouhani, L. Dobrzynski, M. Kushwaha, and P. Halevi, "Complete acoustic band gaps in periodic fibre reinforced composite materials: The carbon/epoxy composite and some metallic systems," J. Phys. Condens. Matter **6**, 8759 (1994).

[3]Z. Liu, X. Zhang, Y. Mao, Y. Y. Zhu, Z. Yang, C. T. Chan, and P. Sheng, "Locally resonant sonic materials," Science **289**, 1734 (2000).

[4]J. O. Vasseur, P. Deymier, B. Chenni, B. Djafari-Rouhani, L. Dobrzynski, and D. Prevost, "Experimental and theoretical evidence for the existence of absolute acoustic band gaps in two-dimensional solid phononic crystals," Phys. Rev. Lett. **86**(14), 3012–3015 (2001).

[5]A. Khelif, P. A. Deymier, B. Djafari-Rouhani, J. O. Vasseur, and L. Dobrzynski, "Two-dimensional phononic crystal with tunable narrow pass band: Application to a waveguide with selective frequency," J. Appl. Phys. **94**, 1308 (2003).

[6]J. O. Vasseur, P. A. Deymier, B. Djafari-Rouhani, Y. Pennec, and A. Hladky-Hennion, "Absolute forbidden bands and waveguiding in two-dimensional phononic crystal plates," Phys. Rev. B **77**(8), 085415 (2008).

[7]N. Fang, D. Xi, J. Xu, M. Ambati, W. Srituravanich, C. Sun, and X. Zhang, "Ultrasonic metamaterials with negative modulus," Nat. Mater. **5**(6), 452–456 (2006).

[8]A. Sukhovich, B. Merheb, K. Muralidharan, J. O. Vasseur, Y. Pennec, P. A. Deymier, and J. Page, "Experimental and theoretical evidence for subwavelength imaging in phononic crystals," Phys. Rev. Lett. **102**, 154301 (2009).

[9]M. Kafesaki, M. M. Sigalas, and N. Garcia, "Wave guides in two dimensional elastic wave band-gap materials," Phys. B Condens. Matter **296**(1-3), 190–194 (2001).

[10]J. Bucay, E. Roussel, J. O. Vasseur, P. A Deymier, A.-C. Hladky-Hennion, Y. Pennec, K. Muralidharan, B. Djafari-Rouhani, and B. Dubus, "Positive, negative, zero refraction, and beam splitting in a solid/air phononic crystal: Theoretical and experimental study," Phys. Rev. B **79**, 214305 (2009).

[11]N. Swinteck, J.-F. Robillard, S. Bringuier, J. Bucay, K. Muralidharan, J. O. Vasseur, K. Runge, and P. A. Deymier, "Phase-controlling phononic crystal," Appl. Phys. Lett. **98**, 103508 (2011).

[12]J. M. Owens and G. F. Sallee, "Surface acoustic wave logic gates," Proc. IEEE **59**(2), 308–309 (1971).

[13]K.-S. Wu, J.-W. Dong, D.-H. Chen, X.-N. Luo, and H.-Z. Wang, "Sensitive photonic crystal phase logic gates," J. Mod. Opt. **96**, 1895–1898 (2009).

[14]J. Bai, J. Wang, J. Jiang, X. Chen, H. Li, Y. Qiu, and Z. Qiang, "Photonic not and nor gates based on a single compact photonic crystal ring resonator," Appl. Opt. **48**, 6923–6927(2009).

[15]M. S. Kushwaha, B. Djafari-Rouhani, L. Dobrzynski, and J. O. Vasseur, "Sonic stop-bands for cubic arrays of rigid inclusions in air," Eur. Phys. J. B **3**(2), 155–161(1998).

[16]M. Sigalas and N. Garcia, "Theoretical study of three dimensional elastic band gaps with the finite-difference time-domain method," J. Appl. Phys. **87**(6), 3122 (2000).

[17]D. Garcia-Pablos, M. Sigalas, F. R. Montero de Espinosa, M. Torres, M. Kafesaki, and N. Garcia, "Theory and experiments on elastic band gaps," Phys. Rev. Lett. **84**, 4349 (2000).

[18]G. Mur, "Absorbing boundary conditions for finite-difference approximation of the time-domain electromagnetic-field equations," IEEE Trans. Electromagn. Compat. **EMC-23**(4), 377–382 (1981).

[19]A. P. Godse and D. A. Godse, *Digital Logic Circuits* (Technical Publications Pune, Pune, India, 2010), Chap. 3, p. 7.